Composites Part B 91 (2016) 431–440

Contents lists available at ScienceDirect

Composites Part B

journal homepage: www.elsevier.com/locate/compositesb

An investigation of hygrothermal effects on adhesive materials and double lap shear joints of CFRP composite laminates

Shufeng Liu [a], Xiaoquan Cheng [a,*], Qian Zhang [a], Jie Zhang [a], Jianwen Bao [b], Xin Guo [a]

[a] *School of Aeronautic Science and Engineering, Beihang University, Beijing, China*
[b] *Beijing Institute of Aeronautical Materials, Beijing, China*

ARTICLE INFO

Article history:
Received 7 September 2015
Received in revised form
27 January 2016
Accepted 29 January 2016
Available online 8 February 2016

Keywords:
B. Adhesion
B. Environmental degradation
D. Mechanical testing
C. Finite element analysis (FEA)

ABSTRACT

This paper was aimed to investigate the hygrothermal effects on the mechanical behavior of the double lap shear joints of Carbon/Epoxy composite laminates, which were bonded using epoxy adhesive film SY14. First, experimental method was used to evaluate the hygrothermal dependent properties of the adhesive and the static response of composite laminate double lap joints at various environment conditions. The specimens were grouped into room temperature/dry (RD), room temperature/wet (RW), elevated temperature/dry (ED) and elevated temperature/wet (EW). The wet specimens were immersed in deionized water at temperature of 90 °C for 60 h and the elevated temperature is 95 °C. Tensile tests were carried out at room temperature and elevated temperature (95 °C) in a controlled chamber. Results showed that the elastic modulus and tensile strength decreased about 24% and 27% respectively after exposure to humidity environment. And a large degradation was found when exposure to high temperature while the plasticity became notable. The failure modes of the double lap shear joints were studied by visual inspection. It was found that both adhesive and cohesive failure happened for dry specimens at room temperature. While failure modes were dominated by cohesive failure after moisture exposure and adhesive failure at elevated temperature. Second, a finite element model was utilized to simulate the damage evolution of the double lap joints. The moisture diffusion process, swelling stress and thermal stress were included. And hygrothermal dependent cohesive law was considered to study the damage evolution. It revealed that failure modes were highly dependent on the weaker strength of adhesive and cohesive. Moisture absorption caused large degradation in cohesive strength, so the failure modes were mostly cohesive failure. Elevated temperature decreases strength of adhesive seriously, so adhesive failure dominates. Good agreement was achieved between the predicted failure loads and experimental results. And the predicted failure modes were also consistent with the experimental phenomenon.

1. Introduction

As more and more polymer reinforced composite materials are used in many aspects of modern applications, such as construction, automotive, ship, aerospace and sports. Traditional mechanical joints are being replaced by adhesively bonded joints partially for the advantages of higher join efficiency, corrosion resistance and lower weight increment, especially in aircraft structures. For aerospace application, there has been a growing requirement for adhesive to stand extreme service environment, such as high temperature and moisture. To ensure the safety of the adhesively joint structures, the adhesive must operate in this hostile environment and sustain the integrity and strength at a certain rate. The durability of adhesive joints under hygrothermal environment has become a big challenge of its application in aerospace industries.

Many studies have been carried out on the shear strength and interfacial fracture toughness of adhesively bonded joints. While a few research work were reported about the hygrothermal effects on the properties of adhesively bonded joints.

Firstly, the hygrotermal dependent properties of adhesive materials should be considered. Temperature-dependent non-linear behavior of a ductile adhesive were evaluated through tensile/

* Corresponding author. School of Aeronautic Science and Engineering, Beihang University, 37 Xueyuan Road, Haidian District, Beijing 100191, China. Tel.: +86 01082338215.

E-mail address: xiaoquan_cheng@buaa.edu.com (X. Cheng).

http://dx.doi.org/10.1016/j.compositesb.2016.01.051
1359-8368/

compression-shear tests on modified Arcan specimens under a wide temperature range by Badulescu et al. [1]. And an exponential Drucker-Prager yield allows a good representation of the non-linear behavior of adhesive. Moreover, a temperature-dependent model can be built by taking into account a linear evolution of the material parameters with respect to the temperature. Based on the mixed modulus concept, Marques et al. [2] suggested mixed adhesive joints to improve the performance of the joints over a wide temperature range. Loh et al. [3] conducted tests on a rubber toughened epoxy adhesive material after exposure a range of moisture conditions, which revealed that the elastic modulus reduced 38% and ultimate tensile strength decreased almost 53% over the moisture range. The degradation is due to the plasticization by the water absorption and disruption of hydrogen bonds between molecular chains in the adhesive.

Ozela et al. [4] investigated the strength of adhesively bonded joints with different adherends, the joint strengths of unidirectional [0] laminates showed higher joint strength than the cross-ply [0/90] laminates and angle-ply laminates [45/-45], but lower than the quasi-isotropic laminates. Composite–composite single lap joints have much higher strength than the aluminum–aluminum joints. Knighta et al.'s [5] study showed that composite single shear lap joints lost approximately 43% of apparent shear strength after hygrothermal aging, including both humidity and elevated temperature. Zhang's test results [6] also showed that the strength of aluminum–aluminum single lap joint barely decreased after hygrothermal aging at ambient humidity, and degraded greatly at high moisture with high temperature. Effect of humidity-temperature cycling on shear and tensile strength of multi-material adhesive joints was studied by Korta et al. [7] and serious degradation of the joints was found even subject to moderately harsh conditions. Park et al. [8] compared strength of composite joints under three environmental conditions. The results showed that the elevated temperature/wet condition improves the joint strengths while the cold temperature/dry decreases the strengths of joints, which was opposite to the above reports. Je Hoon Oh [9] investigated effects of temperature on the torsion strength of tubular composite adhesively bonded joints. Since the coefficients of thermal expansion and stiffness of adhesive and adherends are different, the internal thermal stress plays an important role in predicting the joint strengths under elevated temperature condition. Unlike isotropic adherends, the stacking angles at the bonding surface have considerably influences on the internal thermal stress and joint strength.

A lot of studies focused on the interfacial properties along the bonding area of adhesively bonded joints, including experimental and numerical studies. Li [10] investigated the debonding behavior of composite joints in a bonded double cantilever beam configuration using cohesive zone model and the parameters for cohesive traction-separation law were discussed. Fernandes [11] conducted the end notched flexure (ENF) test to obtain mode II cohesive laws of carbon/epoxy composite bonded joints and the relationship between fracture energy and the crack tip opening displacement in mode II was considered. Loh et al. [12] investigated the moisture dependent interfacial fracture energy of the adhesive/steel interface through mixed mode flexure (MMF) tests and notched coating adhesive (NCA) tests subjected to a range of moisture exposure conditions. For both the two tests, fracture energy reduced from about 770 J/m^2 (740 J/m^2) in dry condition to less than 100 J/m^2 under moisture condition. Experimental investigation was also conducted on the fracture of adhesive dissimilar-material joints under mode-I loading. Double cantilever bending test were conducted on the CFRP/Aluminum adhesively joints to evaluate the mode I fracture strain energy release rate of this dissimilar adherend bonding joints [13]. The fracture toughness of adhesive bonded joints around the glass transition temperature was tested by Banea et al. [14]. It revealed that increasing temperature reduced its strength but enhanced the ductility. Below the glass transition temperature, the mode I fracture toughness is relatively insensitive to temperature. But there comes a drastic decrease when temperature is above glass transition temperature. Despite the composite matrix and adhesive materials are epoxy resins, the latter one has larger mode I fracture toughness but lower interfacial strength [15]. For adhesively bonded joints, the cracks may propagate along paths outside the symmetry plane and fiber bridging generates subsequently along the path. Fracture toughness along different paths were investigated by Shahverdi et al. [16] and it turned out that fiber bridging contribute more to the fracture toughness of mode I crack and less to mode II crack.

The measurement of cohesive properties is always a tough issue for the highly non-uniform stress distributions around the crack tip. Svensson et al. [17] conducted fracture mechanics tests and proposed an inverse method based on FE-simulations to define the cohesive laws and provide the values of the facture energy, the critical separation and the interlaminar strength. Campilho et al. [18] utilized the trapezoidal softening law and mixed mode cohesive damage model to simulate the damage onset and growth of cohesive element, which were used to model the interface between the adhesive and patch and parent laminates. He used this method to predict failure load and failure mechanism of strap repaired composite laminates. Fracture toughness of composite bonded joints subject to mode I, II and mixed mode I + II loading conditions was evaluated by Floros [19] and the joints attained with film adhesive and paste adhesive were compared, which showed the former one has much larger fracture toughness. Based on Mortenson's unified approach, Zhang [20] established a robust and rapid analytical method for 3D stress analysis of composite bonded joints. It can be used to handle with the hygrothermal loads and compute the in-plane and out-of-plane, through-thickness interlaminar peer and shear stress. And the nonlinearity of the adhesive material can be effectively considered in the model. Crocombe [21] studied the moisture dependent strength of single lap joints of steel plates. A numerical model considering moisture mass diffusion process and moisture dependent properties of bulk adhesive and interfacial fracture properties. The interfacial diffusion coefficient was also introduced and gave more accurate prediction of the degraded failure strength of single lap joints exposed to humidity environment.

However, little research was carried out on the mechanical behavior of composite laminates adhesively bonded structure after exposure to humidity and elevated temperature. And the hygrothermal dependent cohesive zone properties were barely reported. This paper focused on the hygrothermal effects on the strength of double lap joints of composite laminates and failure mechanism at various environment conditions. Experimental studies were first carried out to test the mechanical properties of bulk adhesive and double lap joints at four different environment conditions, which were room temperature/dry (RD), room temperature/wet (RW), elevated temperature/dry (ED) and elevated temperature/wet (EW). The cohesive properties at various environment conditions were estimated according to the corresponding adhesive properties. And then, the hygrothermal dependent properties of adhesive and cohesive were then incorporated into the finite element model to predict failure loads and damage evolution of the double lap shear joints at various environment conditions.

2. Materials and specimen manufacture

In this study, an epoxy type adhesive film SY14 provided by Beijing Institute of Aeronautical Materials was used as adhesive.

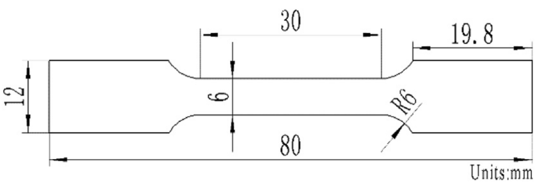

Fig. 1. Configuration of the adhesive dog bone specimen.

The average thickness of SY14 adhesive film is 0.13 mm and its areal density is 159 ± 12 g/m^2. Unidirectional laminates $[0]_{16}$ and $[0]_{32}$ made from T800/5228E prepregs were used as adherends.

To obtain the properties of adhesive materials, tensile specimens were manufactured and tensile tests were conducted under different hygrothermal environment conditions to measure elastic modulus and strength. A plate of the bulk adhesive SY14 was made by 8 layers of the adhesive films curing in an oven. The oven temperature was increased from room temperature (about 22 °C) to 80 °C and maintained at 80 °C for 30 min, and then increased to 180 °C and kept constant for 2 h. During the curing process, a vacuum pressure of 980 mbar was applied. To avoid residual thermal stress in the film, a slow cooling rate was achieved by turning off the oven and keeping the specimen in the oven (with the door shut) for enough time. The adhesive bulk plate was cut into dog bone specimens (see Fig. 1).

The double lap shear joints (DLSJ) specimens were fabricated according to ASTM standard D3528 [22] and were designed as shown in Fig. 2. The middle adherends laminates and the doublers were cut from a 3.2 mm thick panel and a 1.6 mm thick panel, respectively. The overlap length and overlap width were both 25 mm. Each substrate was 110 mm long and the spacers are 3.2 mm thick and 35 mm long. All the panels were cured in autoclave under 180 °C with a pressure of 0.6 MPa and then were cut into the prescribed configurations. Abrasive papers #300 were used to grind the laminates' surface of the bonding area for secondary bonding process. Subsequently, the bonding surface was cleaned using acetone. After the drying of the laminates, they were bonded together with adhesive film SY14 and fastened by AIRTEC blue tapes to prevent the sliding of adherends and maintain the bonding surface. Then, the bonded laminates were put into a vacuum bag and the cured in an oven at 180 °C using the same curing process of the adhesive film as above. The average thickness of the adhesive layer after cured was approximately 0.1 mm.

3. Experimental tests

3.1. Specimen aging

To investigate the hygrothermal environment's effects on the properties of the adhesive (i.e. the elastic modulus and tensile strength), the dog bone specimens of bulk adhesive were immersed in deionised water at 90 °C for 60 h. The gravimetric method was used to measure the coefficient of moisture diffusion and equilibrium moisture uptake. At the same time, thickness measurements were performed using a micrometre with 0.001 mm accuracy to investigate the swelling of bulk adhesive during water absorption. Only the thickness was measured with assumption that the swelling was isotropic. And the DLSJ specimens were also immersed in water at 90 °C water for 60 h to simulate wet condition.

3.2. Mechanical tests

The static tensile tests of bulk adhesive were performed using an Instron test machine (20 kN servo-hydraulic test machine). An extensometer with a maximum measurement range of 2.5 mm was used to measure the elongation of the bulk specimen. The test rate was 0.5 mm/min. The experiments were grouped into four types: RD (room temperature/dry), RW (room temperature/wet), ED (elevated temperature/dry) and EW (elevated temperature/wet). The elevated temperature was 95 °C. ED and EW test groups were conducted in a controlled chamber (see Fig. 3a). For each group, five dog bone specimens were tested and there were 20 specimens in total.

For DLSJ specimens, the tests were conducted using another Instron test machine 8801 with a load cell of 100 kN and a controlled chamber. An extensometer was used to test the deformation, i.e. the relative displacement between the adherends (see Fig. 3b). The load was applied at a crosshead speed of 1.25 mm/min based on the ASTM D3528 specifications. DLSJ specimens were also divided into four groups according to the environment conditions and each group had five specimens.

4. Results and discussion

4.1. Bulk adhesive tensile tests

The tensile test results of bulk adhesive plates were mainly focused on the elastic modulus and tensile strength of the adhesive materials. As shown in Fig. 4, the tensile stress versus strain curves under different environmental conditions were compared, showing the hygrothermal environment condition has a considerable influence on properties of the adhesive materials. After immersing in water 60 h, the elastic modulus decreased approximately 23.6%, and the tensile strength reduced 27%. While at elevated temperature, a dramatic drop in both modulus and tensile strength happened, but the plasticity became more notable. A summary of the properties of adhesive materials was listed in Table 1.

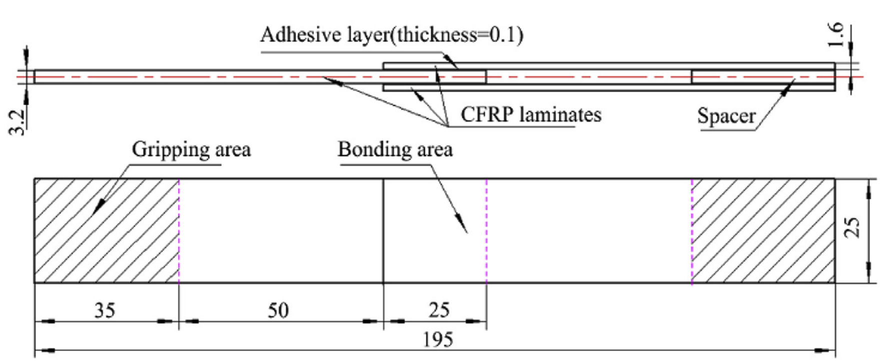

Fig. 2. Configuration of DLSJ specimen.

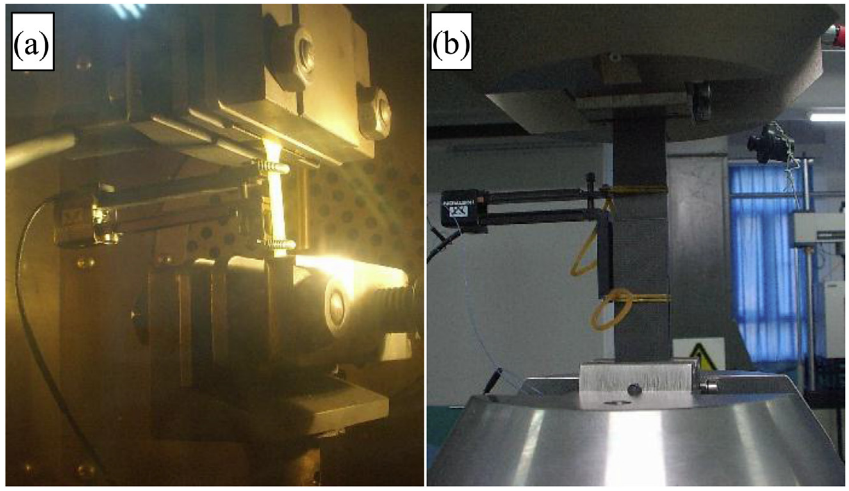

Fig. 3. Test set-up for (a) adhesive dog bone specimen test at controlled chamber (b) DLSJ specimen.

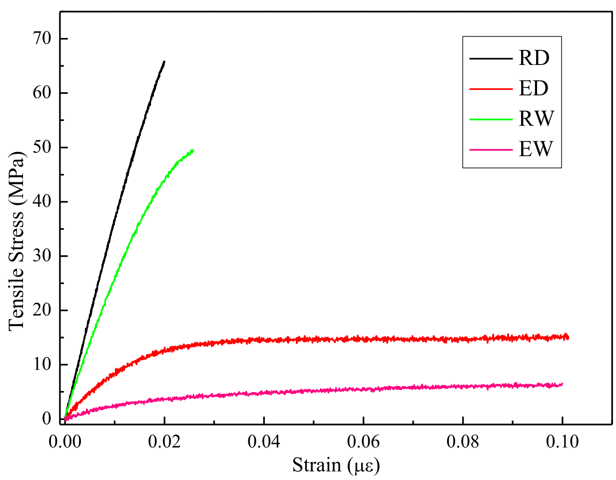

Fig. 4. Stress–strain curves of adhesive at four environment conditions.

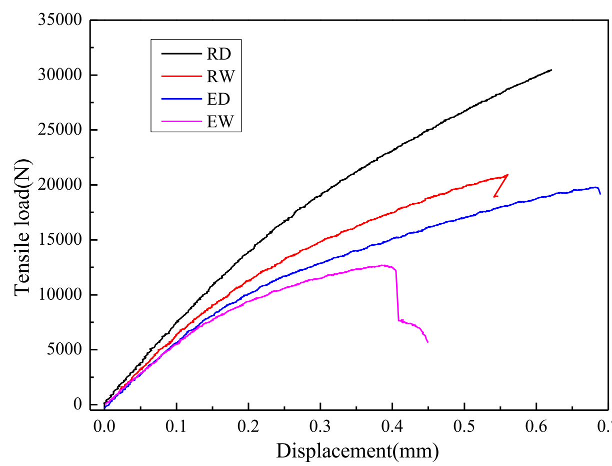

Fig. 5. Load–displacement curves of DLSJ specimens at four environment conditions.

4.2. The double lap shear joints

Fig. 5 gives the load–displacement curves of the DLSJ specimens under uniaxial loading in four different environmental conditions. As can be easily seen, the joint strength decreased almost 31.3% after immersing in water for 60 h, and dropped 27.7% and 54.4% in ED and EW environment, respectively. It indicates that the humidity environment has non-ignorable influences on the joint strength of composite DLSJ specimens, and moreover, the elevated temperature can be a deleterious factor to the performance of adhesively bonded structures. The failure modes corresponding to the four environment conditions were different. Typical failure modes of the four test groups were shown in Fig. 6. For RD Group, the failure modes consisted of almost 70% cohesive failure and 30% adhesive failure. And cohesive failure modes dominated the RW and EW Groups, while adhesive failure dominated the ED Group. Table 2 gives a summary of the overall test results of the four test groups, in which the nominal shear strength is the failure load divided by bonding area. The bonded area is double the product of measured overlap length and width.

5. Finite element modelling (FEM)

5.1. Moisture diffusion

The moisture diffusion procedure of the CFRP DLSJ specimens immersing in water with a temperature of 90 °C was modelled using the mass diffusion module of Abaqus 6.11. The moisture diffusion behavior of laminate and adhesive material was simulated

Table 1
Summary of the adhesive's properties at four environment conditions.

Group	RD	RW	ED	EW
Elastic modulus (MPa)	3730 ± 260	2810 ± 70	1140 ± 0.13	268.38 ± 14
Tensile strength (MPa)	65.92 ± 3.6	47.52 ± 3.1	21.85 ± 2.69	9.82 ± 1.5
Elongation at breakage (%)	1.96	2.32	–	–

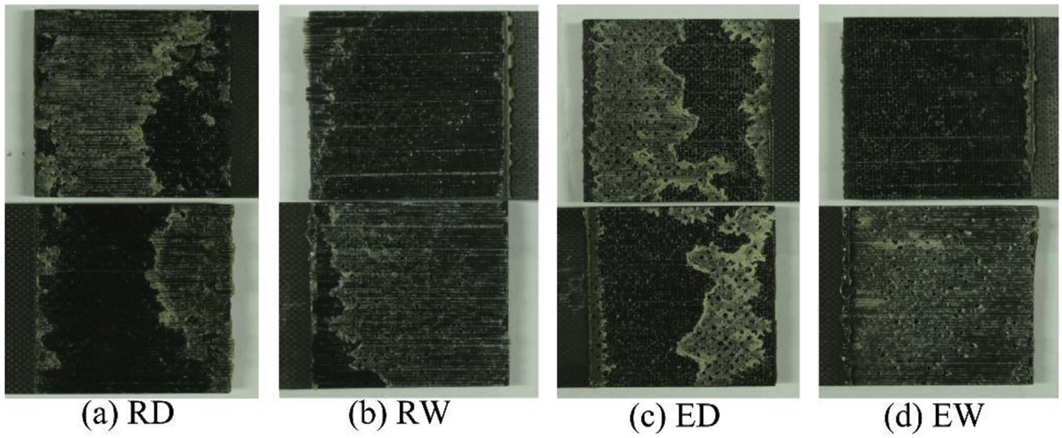

Fig. 6. Demonstration of the failure modes of the four groups.

Table 2
A summary of the static response of the DLSJ specimens at four environment conditions.

Test group	Average failure load (kN)	Nominal shear strength (MPa)	Failure modes*
RD	27.45 ± 2.65	21.36 ± 2.20	a
RW	19.09 ± 1.77	14.66 ± 1.26	b
ED	20.24 ± 1.38	15.45 ± 1.10	c
EW	12.76 ± 0.78	9.75 ± 6.38	b

*a represents both adhesive and cohesive failure; b represents cohesive failure; c represents mostly adhesive failure and partially cohesive failure.

following the Fickian's second law [23], according to which the temporal and spatial moisture concentration(c) at time t is expressed as:

$$\frac{\partial c(z,t)}{\partial t} = D_z \frac{\partial^2 c(z,t)}{\partial^2 z} \quad (0 \le z \le h, \quad t > 0) \tag{1}$$

$$c = c_i \quad (0 < z < h, \quad t \le 0)$$

$$c = c_\infty \quad (z = 0 \quad \text{or} \quad z = h, \quad t > 0)$$

where D_z is the Fickian diffusion coefficient in thickness direction, h is the plate's thickness, c_i and c_∞ were initial moisture concentration and maximum equilibrium moisture concentration respectively.

As the moisture diffusion procedure was symmetrical, half the model was established. As seen in Fig. 7, a 3D model was used and the bonding area was simulated by two cohesive layer and one adhesive layer. For moisture diffusion analysis, the model was meshed using DC3D8 element type. As the moisture ingresses from all outside surfaces, the mass concentration was specified to be 1.0 on all the outside surfaces. The moisture diffusion parameters of adhesive material was determined through gravimetric measurements. Whereas, the diffusivity of laminates was obtained according to literature [24] and the handbook [25]. The moisture diffusivity perpendicular to fiber direction is defined as a function of temperature, see Equation (2) [24].

$$D = 0.57 \exp(-4993/T) \tag{2}$$

where T is temperature and unit is K. And the moisture diffusivity along the fiber direction is estimated 1.85 times the transverse diffusivity [26]. The diffusion parameters of composite laminates and adhesive material were listed in Table 3.

As shown in Fig. 8a, the moisture concentration at the middle cross section at different time was described. And Fig. 8b showed the final internal overall moisture distribution. It can be seen that

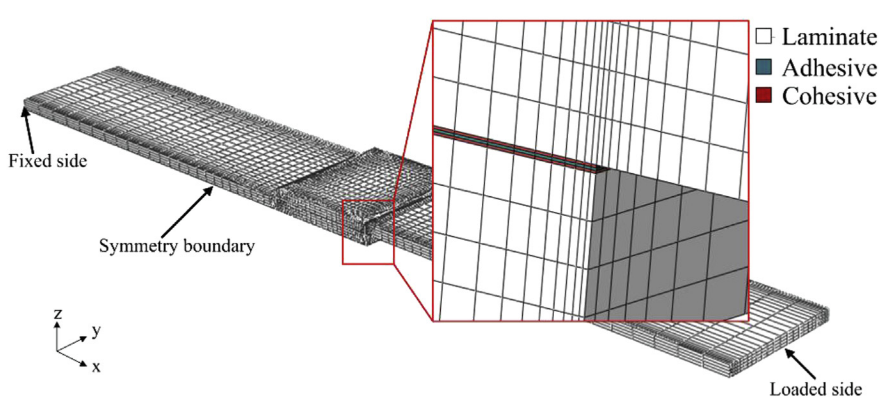

Fig. 7. Boundary conditions and meshing of the DLSJ.

Table 3
Moisture diffusion characteristics of the CFRP composite laminates and adhesive.

Material		Diffusivity (mm^2/s)	Equilibrium concentration (g/mm^3)	Density (g/mm^3)
Laminates	$D_{\parallel}$	5.6×10^{-7}	2.52×10^{-5}	1.68×10^{-3}
	$D_{\perp}$	2.9×10^{-7}		
Adhesive		6.28×10^{-6}	8.13×10^{-5}	1.2×10^{-3}

$D_{\parallel}$: Diffusivity parallel to fiber direction.
$D_{\perp}$: Diffusivity perpendicular to fiber direction.

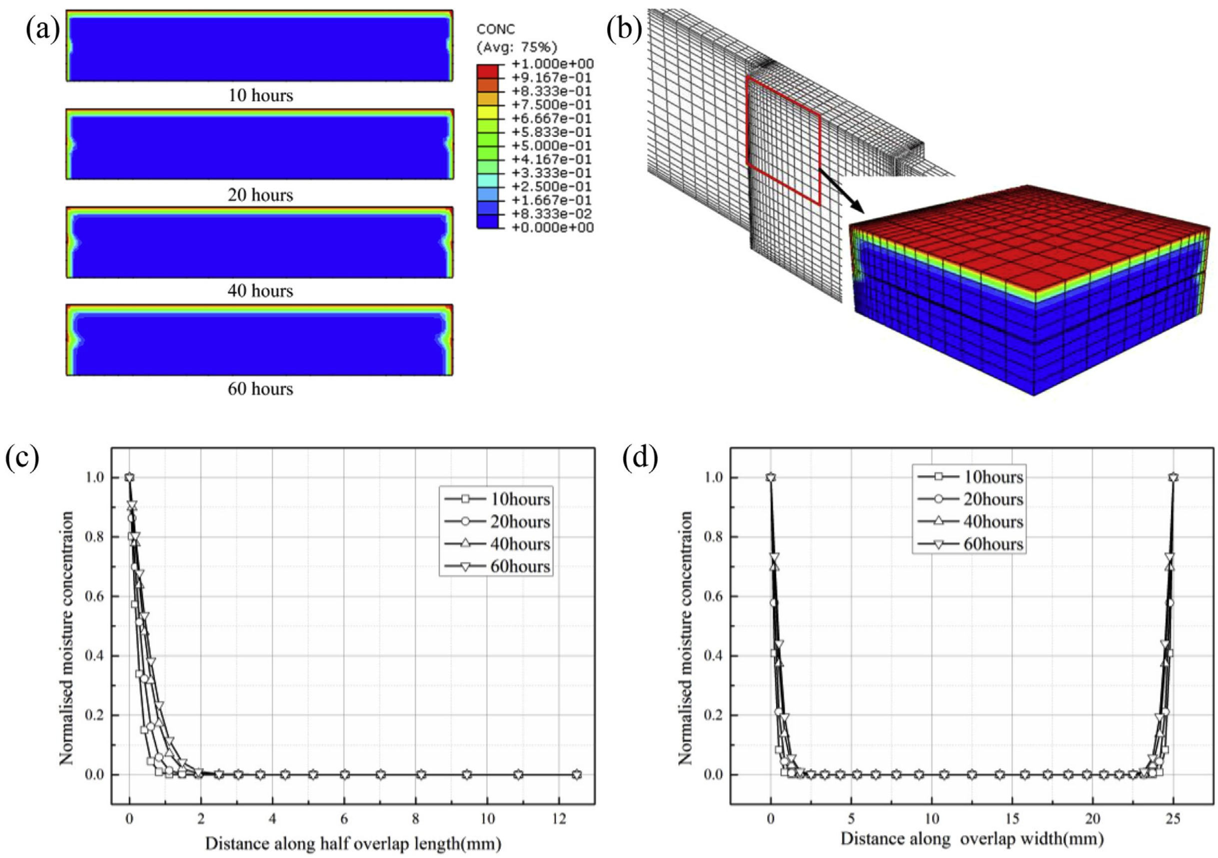

Fig. 8. (a) moisture concentration distribution in the middle cross-section during the diffusion procedure (b) the internal overall moisture concentration distribution (c) normalized moisture concentration in the middle of the adhesive layer along half the overlap length and (d) the overlap width.

the moisture diffused faster in the adhesive layer. The normalized moisture concentration in the middle plane of the adhesive layer along the half overlap length and width were displayed in Fig. 8c and d, respectively.

5.2. Hygrothermal stress–strain relation [27]

The strain induced by thermal expansion and swelling can be expressed as:

$$\{\varepsilon\} = [S]\{\sigma\} + \{\beta\}\Delta C + \{\alpha\}\Delta T \tag{3}$$

So the constitutive law of hygrothermal elasticity is given below:

$$\{\sigma\} = [Q](\{\varepsilon\} - \{\beta\}\Delta C - \{\alpha\}\Delta T) \tag{4}$$

where $[S]$ is the compliance matrix and $[Q]$ is the stiffness matrix; $\{\alpha\}$ and $\{\beta\}$ are thermal and moisture expansion coefficient vector respectively; ΔT is the temperature rise and ΔC is the increase in moisture concentration (%). If (T_0, C_0) are the reference hygrothermal state, then the change in temperature is expressed as $\Delta T = T - T_0$ and the change in moisture concentration $\Delta C = C - C_0$.

After the diffusion analysis, the spatial moisture concentration was transferred to a field variable and output into a result file (.fil) for hygrothermal stress analysis. The moisture strain cannot be calculated directly but should be analyzed through the thermal stress analysis for they have similar expansion behavior. Before reading the result file for predefined temperature field, the data form structure of the result file was converted through a post-processing program. The swelling strain was computed as a product of CME (coefficient of moisture expansion) and moisture concentration (stored as TEMP). In order to consider effects of both temperature and humidity, the thermal strain was also computed as a product of CTE (coefficient of thermal expansion) and the temperature drop (ΔT) and incorporated with swelling strain. Same mesh was used for hygrothermal stress analysis, but the element type was converted to C3D8R for laminates and adhesive layer and COH3D8 for cohesive layer.

The CME of adhesive based epoxy systems have been found to be 0.0016–0.01/wt% moisture uptake [28]. In this work, the

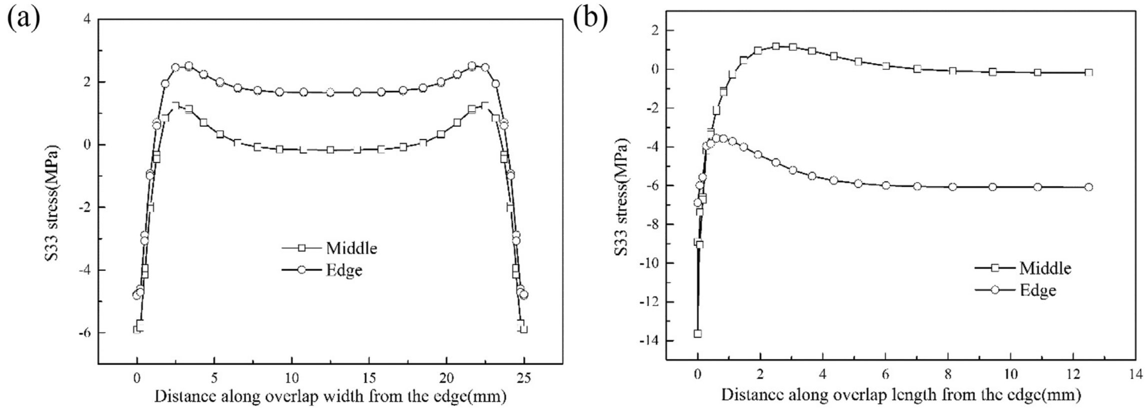

Fig. 9. Moisture swelling induced stress in the adhesive along thickness direction, (a) along overlap width and (b) half overlap length.

swelling coefficient was measured as 0.0064/wt%. And the CME of composite laminates were also orthotropic: the longitudinal and transverse CME β_{11}, β_{22} were 2.5×10^{-8}/wt% and 0.001/wt%, respectively, which were similar to those used in Refs. [24,27,29]. The CTE of laminates parallel to and perpendicular to fiber direction were 0.10×10^{-6}/K and 26.0×10^{-6}/K, respectively. And the CTE of adhesive was 40×10^{-6}/K.

The inner stress were plotted on paths located on the mid-plane of the bond line; aligned along the edge and middle of the overlap in both overlap width and overlap length. Figs. 9 and 10 showed the stress induced by swelling and thermal expansion, respectively. It indicated that the stress S33 was largest at the peripheral region of the overlap. And compressive stress developed at the edge of the overlap for the higher swelling of adhesive at the region. While the thermal induced stress was relatively small for the reason that elevated temperature caused large degradation of the adhesive's elastic modulus.

5.3. Static response of double lap joints of composite laminates

After the hygrothermal stress analysis, a static strength analysis was conducted by applying a displacement at the right side as shown in Fig. 7. The elastic properties of the composite laminates used were listed in Table 4. As observed from the experimental tests, there were no failure in laminates and the DLSJ specimens lost their strength all due to the failure of adhesive or interface. Although the mechanical properties of the laminates degrade at the hygrothermal conditions, it had little influence on the failure load of the joints because the failure was localized at the bondline. So the degradation of the laminate's mechanical property was ignored in this analysis. Also, the strength of the laminates were checked in this model and it proved no failure appeared in the laminates while the joints lost their loading capacity. Therefore, no damage was considered for laminates in this model.

The cohesive zone element were used between the laminates and adhesive materials, representing the interfaces between laminates and adhesive. The bi-linear traction-separation law was employed for the cohesive zone element to predict the progressive damage of the cohesive interface. To simulate the failure of the adhesive film, maximum shear criterion was used.

$$\tau_{\max} = (\sigma_1 - \sigma_3)/2 \geq S \tag{5}$$

where σ_1 and σ_3 are the maximum and minimum principal stresses and S is the shear strength of the adhesive. Once the failure is detected, the modulus of the adhesive is degraded to zero. But for the sake of convergence, it is replaced by a very small value of 0.01.

As discovered in previous researches [14,28], the adhesive and cohesive interface properties were highly dependent on the hygrothermal environment. In this work, the properties of adhesive were obtained through the bulk adhesive tests. The cohesive zone properties (i.e. the normal and shear critical tractions, stiffness and fracture energies) were reduced as the environment condition, as shown schematically in Fig. 11.

To quantify the cohesive zone properties, a simple assumption was made that the properties of adhesive and cohesive zone were

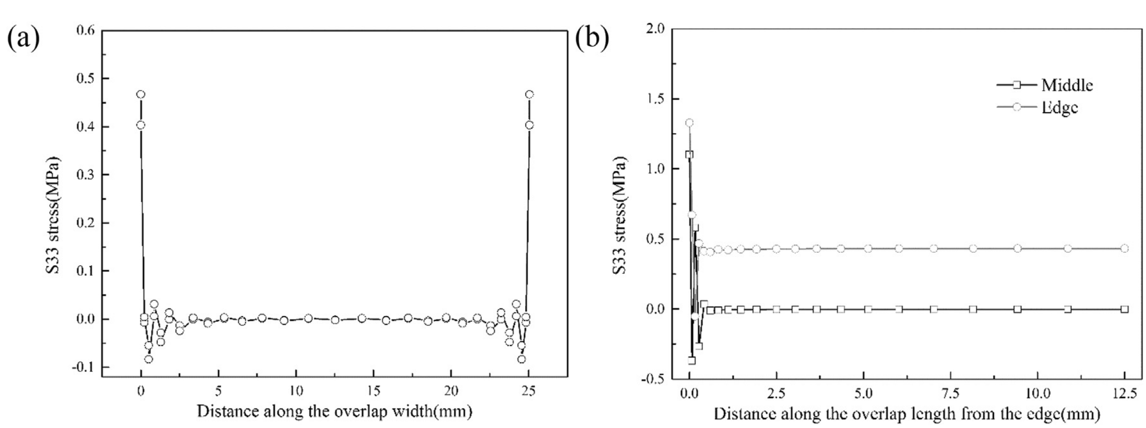

Fig. 10. Thermal induced stress in the adhesive along thickness direction (a) along overlap width in the middle cross section of the adhesive and (b) along half the overlap length.

Table 4
Properties of the laminate.

Elastic modulus in fiber direction, E_{11} (GPa)	172
Elastic modulus in transverse direction, E_{22} (GPa)	8.1
Elastic modulus in normal direction, E_{33} (GPa)	8.1
Shear modulus, G_{12} (GPa)	5.6
Shear modulus, G_{13} (GPa)	5.6
Shear modulus, G_{23} (GPa)	3.9
Poisson's ratio, ν_{12}	0.32
Poisson's ratio, ν_{13}	0.32
Poisson's ratio, ν_{23}	0.35

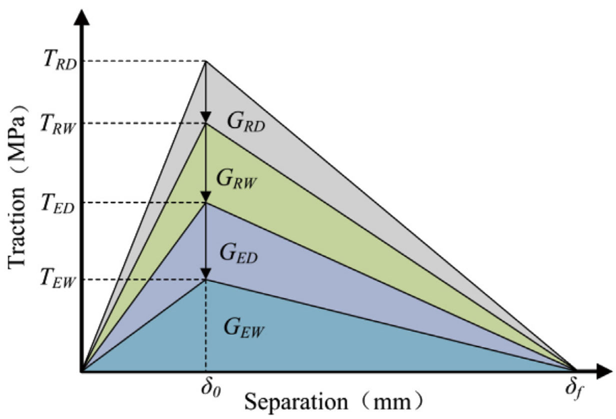

Fig. 11. Schematic of degradation of bilinear traction-separation model due to hygrothermal conditions.

degraded by multiplying an estimated factor according to the four environment conditions respectively. And the degrading factors were estimated by the square root of degradation proportion of the adhesive material's elastic modulus and strength. When subjected to humidity environment, the interface strength was degraded more by multiplying an extra factor (see Equation (6)). And in this work, the factor f was empirically valued as 0.6.

$$T^h = T_0 \cdot \sqrt{\frac{\sigma^h}{\sigma}} \cdot f \tag{6}$$

where T^h and T_0 are critical traction with and without moisture absorption; σ^h and σ are ultimate strength of adhesive with and without moisture absorption, which can be obtained from experimental tests; and f is the extra degrading factor.

The properties of adhesive and cohesive under the four environment conditions were listed in Table 5. The interface stiffnesses of the cohesive element were determined using the following formula from Ref. [30].

$$K_{nn} = \frac{\alpha E}{t}, \quad K_{tt} = K_{ss} = \frac{\alpha G}{t} \tag{7}$$

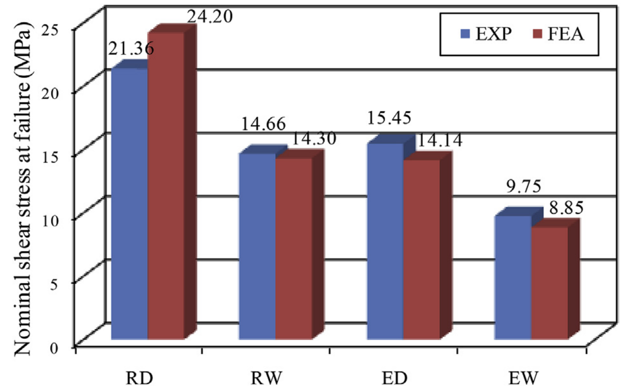

Fig. 12. The average experimental and predicted shear strength of DLSJ at four environment conditions.

where t is the constitute thickness of the cohesive element; E, G are tensile and shear moduli of adhesive, respectively; α is taken as 50. Interface strengths were determined by adhesive's tensile and shear strength. Critical fracture energy release rates of the interface were estimated according to literature [12,21]. And the corresponding interface properties under hygrothermal environment condition were degraded using the method as described above.

As shown in Fig. 12, the finite element model had a good ability in predicting the failure strength of the DLSJ specimens exposed to the four environmental conditions. For the RD group, the predicted nominal shear stress at failure was 24.2 MPa with an error of 13.3%. While the predict results for the RW, ED and EW group had error of −2.4%, -8.4% and −9.2%, respectively. The damage evolution of the cohesive and adhesive layers was shown in Fig. 13. For Group RD, the damage initiated in the left-side edge of the cohesive, and when approximately half the cohesive layer degraded to zero (i.e. SDEG = 1), the fracture transferred to the adhesive (see Fig. 13a). The failure process was the same with the experimental phenomenon. And for Group RW and EW, the failure modes were dominated by cohesive failure (see Fig. 13b and d). The reason could be that the moisture uptake decreased the strength of the cohesive more than the adhesive layer and the cohesive damaged prior to the adhesive. While under elevated temperature, the property of adhesive dropped dramatically which was demonstrated by the experimental tests. Therefore, the failure modes of Group ED were mainly adhesive failure (see Fig. 13c). The failure mechanism obtained from the numerical results was consistent with the experimental observation (see Fig. 6).

6. Conclusions

In this paper, an experimental investigation was carried out on the hygrothermal effects on the mechanical properties of adhesive material and CFRP composite laminates double lap joints. And a

Table 5
Properties of adhesive and cohesive at four environment conditions.

Adhesive			Cohesive					
Condition	E (MPa)	σ_u (MPa)	K_{nn} (N/mm^3)	$K_s = K_t$ (N/mm^3)	T_n (MPa)	$T_s = T_t$ (MPa)	G_{IC} (N/mm)	$G_{IIC} = G_{IIIC}$ (N/mm)
RD	3730	66	112,000	40,000	66	40	1.2	2.5
RW	2800	48	85,000	30,000	33	20	0.53	1.2
ED	1140	21.9	35,000	12,500	38	23	0.7	1.4
EW	300	9.8	13000	5000	15	10	0.3	0.6

E: Young's modulus, σ_u: yielding strength, K_{nn}: interface stiffness in normal direction, K_s and K_t: interface stiffness in two shear directions, T_n: interface strength in normal direction, T_s and T_t: interface strength in two shear directions, G_{IC}, G_{IC} and G_{IIIC}: Mode I, II and III critical fracture energy release rates.

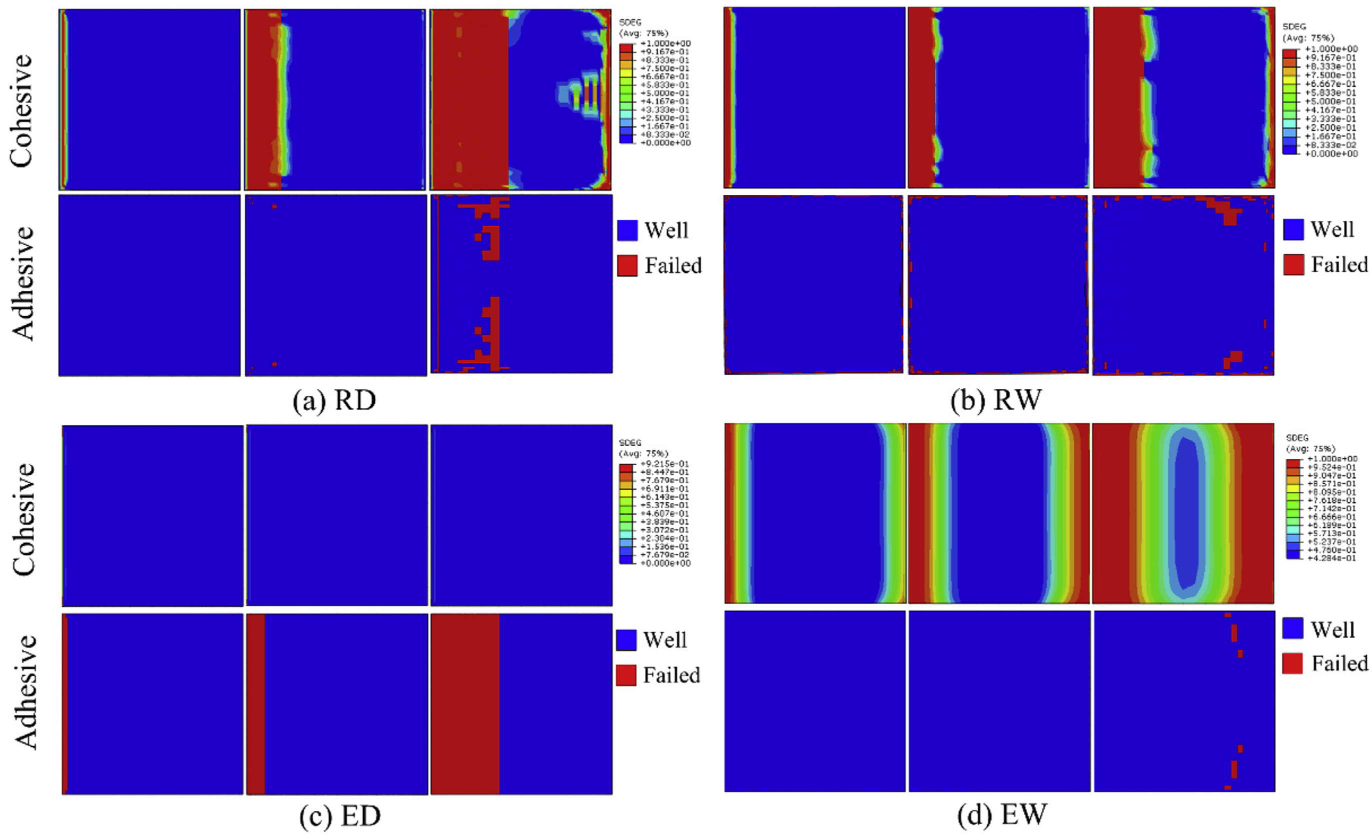

Fig. 13. Predicted failure modes of the adhesive and cohesive under the environment conditions: (a) RD, (b) RW, (c) ED, and (d) EW.

FEM was established to study the failure mechanism of the DLSJ under tensile loading using cohesive zone modelling. The following conclusions can be summarized:

(1) The elastic modulus and tensile strength of the adhesive degraded more when the hygrothermal condition become more serious. After moisture absorption, degradation of tensile strength was greater than that of elastic modulus. And a dramatic drop of both elastic modulus and tensile strength when subjected to elevated temperature, while the plasticity characteristic becomes notable.
(2) The shear strength of the DLSJ specimens decreased approximately 31.3% after moisture absorption, and dropped 27.7% and 54.4% in ED and EW environment, respectively. It indicates the combination of humidity and elevated temperature degraded the structural strength significantly.
(3) For Group RD, the failure modes of the DLSJ specimens consisted of almost 70% cohesive failure and 30% adhesive failure. However, after immersing in 90 °C water for 60 h, the failure modes converted to cohesive failure. When exposed to elevated temperature, adhesive failure dominated the failure modes. But after exposure to both elevated temperature and humidity, the failure mode was mainly cohesive failure. It indicates that degradation of the interface strength caused by the moisture absorption is larger than that of the adhesive's strength subjected to high temperature.
(4) The FEM simulated the moisture absorption process and calculated the stress induced by moisture swelling and thermal expansion. It turned out that the stress was very small and marginally influenced the predict failure load.
(5) An estimation was made in the FEM for the properties of cohesive under the four different environment conditions according to the experimental results of the adhesive's mechanical properties. As the moisture absorption degraded the interface strength more seriously, an extra degrading factor was used empirically. The predicted results showed a good consistency with experimental data. The failure modes are highly dependent on the weaker strength of adhesive and cohesive. The predicted damage evolution showed a good agreement with the experimental phenomenon.

Acknowledgements

Financial support National Natural Science Foundation of China (Grant No.11472024) on this study is gratefully acknowledged. Furthermore, the doctorial innovation fund of Beihang University is also gratefully acknowledged.

References

[1] Badulescu C, Cognard JY, Créac'hcadec R, Vedrine P. Analysis of the low temperature-dependent behaviour of a ductile adhesive under monotonic tensile/compression–shear loads. Int J Adhes Adhes 2012;36:56–64.
[2] Marques EAS, da Silva LFM, Flaviani M. Testing and simulation of mixed adhesive joints for aerospace applications. Compos Part B Eng 2015;74:123–30.
[3] Loh WK, Crocombe AD, Wahab MMA, Ashcroft IA. Modelling anomalous moisture uptake, swelling and thermal characteristics of a rubber toughened epoxy adhesive. Int J Adhes Adhes 2005;25(1):1–12.
[4] Ozel A, Yazici B, Akpinar S, Temiz S. A study on the strength of adhesively bondedan joints with different adherends. Compos Part B Eng 2014;62:167–74.
[5] Knight GA, Hou TH, Belcher MA, Palmieri FL, Wohl CJ, Connell JW. Hygrothermal aging of composite single lap shear specimens comprised of AF-555M adhesive and T800H/3900-2 adherends. Int J Adhes Adhes 2012;39:1–7.

[6] Zhang F, Wang HP, Hicks C, Yang X, Carlson BE, Zhou Q. Experimental study of initial strengths and hygrothermal degradation of adhesive joints between thin aluminum and steel substrates. Int J Adhes Adhes 2013;43:14–25.
[7] Korta J, Mlyniec A, Uhl T. Experimental and numerical study on the effect of humidity-temperature cycling on structural multi-material adhesive joints. Compos Part B Eng 2015;79:621–30.
[8] Park YB, Song MG, Kim JJ, Kweon JH, Choi JH. Strength of carbon/epoxy composite single-lap bonded joints in various environmental conditions. Compos Struct 2010;92(9):2173–80.
[9] Oh JH. Strength prediction of tubular composite adhesive joints under torsion. Compos Sci Technol 2007;67(7):1340–7.
[10] Li G, Li C. Assessment of debond simulation and cohesive zone length in a bonded composite joint. Compos Part B Eng 2015;69:359–68.
[11] Fernandes R, Chousal JAG, de Moura M, Xavier J. Determination of cohesive laws of composite bonded joints under mode II loading. Compos Part B Eng 2013;52:269–74.
[12] Loh WK, Crocombe AD, Wahab MMA, Ashcroft IA. Environmental degradation of the interfacial fracture energy in an adhesively bonded joint. Eng Fract Mech 2002;69(18):2113–28.
[13] Khoshravan M, Mehrabadi FA. Fracture analysis in adhesive composite material/aluminum joints under mode-I loading; experimental and numerical approaches. Int J Adhes Adhes 2012;39:8–14.
[14] Banea MD, da Silva LFM, Campilho RDSG. Effect of temperature on tensile strength and mode I fracture toughness of a high temperature epoxy adhesive. J Adhes Sci Technol 2012;26(7):939–53.
[15] Ducept F, Davies P, Gamby D. Mixed mode failure criteria for a glass/epoxy composite and an adhesively bonded composite/composite joint. Int J Adhes Adhes 2000;20(3):233–44.
[16] Shahverdi M, Vassilopoulos AP, Keller T. Mixed-mode quasi-static failure criteria for adhesively-bonded pultruded GFRP joints. Compos Part A Appl Sci Manuf 2014;59:45–56.
[17] Svensson D, Alfredsson KS, Biel A, Stigh U. Measurement of cohesive laws for interlaminar failure of CFRP. Compos Sci Technol 2014;100:53–62.
[18] Campilho R, De Moura M, Domingues J. Using a cohesive damage model to predict the tensile behaviour of CFRP single-strap repairs. Int J Solids Struct 2008;45(5):1497–512.
[19] Floros IS, Tserpes KI, Löbel T. Mode-I, mode-II and mixed-mode I+ II fracture behavior of composite bonded joints: experimental characterization and numerical simulation. Compos Part B Eng 2015;78:459–68.
[20] Zhang J, Bednarcyk BA, Collier C, Yarrington P, Bansal Y, Pindera MJ. 3D stress analysis of adhesively bonded composite joints. In: Proceedings of the AIAA/ASME/ASCE/AHS/ASC 46th Structures, Structural dynamics, and materials conference, Austin Texas; April, 2005. 2006–1959.
[21] Crocombe AD, Hua YX, Loh WK, Wahab MA, Ashcroft AI. Predicting the residual strength for environmentally degraded adhesive lap joints. Int J Adhes Adhes 2006;26(5):325–36.
[22] ASTM D3528. Standard test method for strength properties of double lap shear adhesive joints by tension loading. West Conshohocken, PA: ASTM International; 2008.
[23] Jedidi J, Jacquemin F, Vautrin A. Design of accelerated hygrothermal cycles on polymer matrix composites in the case of a supersonic aircraft. Compos Struct 2005;68(4):429–37.
[24] Benkhedda A, Tounsi A, Adda bedia EA. Effect of temperature and humidity on transient hygrothermal stresses during moisture desorption in laminated composite plates. Compos Struct 2008;82(4):629–35.
[25] Zhao QS. The handbook of advanced composite materials. China Machine Press; 2003.
[26] Bao LR, Yee AF. Moisture diffusion and hygrothermal aging in bismaleimide matrix carbon fiber composites—part I: uni-weave composites. Compos Sci Technol 2002;62(16):2099–110.
[27] Kundu CK, Han JH. Nonlinear buckling analysis of hygrothermoelastic composite shell panels using finite element method. Compos Part B Eng 2009;40(4):313–28.
[28] Sugiman S, Crocombe AD, Aschroft IA. Experimental and numerical investigation of the static response of environmentally aged adhesively bonded joints. Int J Adhes Adhes 2013;40:224–37.
[29] Kumar R, Lal A, Patil HS, Singh BN. Hygrothermally induced buckling analysis of elastically supported laminated composite plates with random system properties. J Compos Mater 2012;46(21):2711–30.
[30] Turon A, Davila CG, Camanho PP, Costa J. An engineering solution for mesh size effects in the simulation of delamination using cohesive zone models. Eng Fract Mech 2007;74(10):1665–82.